On Application of Entropy Characteristics to Texture Analysis

NATALIA AMPILOVA, IGOR SOLOVIEV
Comp. Sci. Dept.
St. Petersburg State University
University emb, 7/9, St. Petersburg, 199034
RUSSIA
n.ampilova@spbu.ru i.soloviev@spbu.ru

Abstract: - A method of texture analysis based on using the Kullback-Leibler divergence is discussed. A digital image is described by a discrete probability distribution. We consider a group of direct multifractal transforms relating to the distribution and for two given images calculate a vector of Kullback-Leibler divergences between the initial distributions and their direct multifractal transforms. The method is illustrated on the example of the Serpinsky carpet. Numerical experiments were performed for the Brodatz textures and for two classes of biomedical preparation images — healthy kidney and kidney with chronic pyelonephritis. In each class divergence vectors between pairs of images are calculated and then the average divergence vector is formed. This vector is considered as a classification sign for the class. The experiments were performed both in gray scale and HSV palette (component wise) and showed that for different classes average divergence vectors are substantially different in each color component. The method may be successfully applied for classification of biomedical preparation images.

Keywords: - Direct multifractal transform, discrete probability distribution, Kullback-Leibler divergence, texture analysis.

1 Introduction

1.1 Review

The problem of analysis and classification of digital images having structural features (textures) is very important and actual. Regarding textures, literature contains examples of images having both regular and irregular structure. Hence to analyze such images one have to use a number of methods — statistical, fractal, multifractal, morphological, spectral ones.

Any method of textural analysis results in obtaining a numerical characteristic (or a feature set) that may be used as a classifying sign to refer the images under investigations to some classes.

Methods of morphological analysis are based on the concepts of the set theory [8,19]. They allow us to find out objects and contours of different types or localize clusters of pixels having close intensities. Many experimental studies show that morphological approach is appropriate for images with irregular structures (e.g for images of living tissues or viscera images). As a rule, such methods lead to better results when combining with filtration. Now morphological methods are widely used for analysis of MRI and ultrasonic diagnostics images [14], and in combining with segmentation [1].

The structure of any digital image is defined by pixel intensities. One of well-known statistical analysis methods consists in obtaining Gray Level Cooccurence Matrix from the intensity matrix [9,10] and calculation some statistical features (the Haralick characteristics or so called second-order statistics).

Fractal analysis methods are based on the assumption that the number of boxes needed to cover a complex set A is proportional to the box size in a power d. When tending the box size to zero one may obtain a sequence of approximate values for d. The limit of the sequence is called fractal dimension of the set A. The most widely used fractal dimensions are box-counting dimensions and the Minkovsky dimension [6].

But for images with complex structures it may be insufficient to have only fractal dimension as a characteristic. Such images are supposed to be a union of several intertwined fractal subsets, being each of them has its own fractal dimension. This approach leads to multifractal analysis. For a given digital image it is reasonable to relate a measure distribution that describes densities of different parts of the image. With this object in view the image is partitioned on a set of boxes by a given

size, and for every box its measure is calculated. In the simple case the measure of the box is defined as the sum of pixel intensities, but sometimes various filters may be applied [22]. The obtained distribution is normed. The set of fractal dimensions of the subsets forms multifractal spectrum. It may be calculated by the method of direct determination [5] or by using Regny spectrum [21].

It is very often several methods should be applied to classify textural images. For example in [15] to detect mild glaucoma stage the author applies discrete wavelet transform and then calculates statistical signs for obtained wavelet coefficients matrix. The detailed survey and bibliography on this subject are given in [20].

1.2 Entropy characteristics

One can observe that since any digital image may be represented by pixel intensities and a discrete probability distribution, to obtain an image characteristic means to extract the information described by this distribution. In information theory the notion *information* was originally concerned with Shannon entropy. Later A. Regny introduced a set of entropies depending on a real parameter α, which goes into the Shannon entropy when α tends to unity. As it was mentioned in [13], "one of the fundamental observation of information theory is that the most general functional form for the mean transmitted information (i.e., information entropy) is that of Regny". A. Bashkirov [4] also supposed to consider namely Regny entropy as statistical characteristic of complex systems. Moreover, he proved that for systems with power-series distribution the Regny entropies for $\alpha < 1$ are mostly representative. Basing on these entropies one can obtain the Regny spectrum — a set fractal dimensions depending on a real parameter α.

We note that many problems concerning a measure distribution are formulated in entropy terms. Thus, in the paper [7] authors use Regny entropy to distinguish types of polyps images. The authors of [16] consider the image entropy as a characteristic of the image focusing: the minimal entropy value corresponds to the best focusing image.

There is a large class of research tasks that may be formulated by the following way: for given restrictions to find a distribution that maximizes (or minimizes) Regny entropy. Examples of the solution of such problems are given in [4,21].

One more example is connected with a construction of a stationary flow on a graph. Now it is widely accepted that textural images may be considered as phase portraits of complex dynamical systems in some points of time. For dynamical systems various types of invariant sets are subjects of much interest. By analyzing phase portraits we may find so called stationary states of a process, being the existence of such states means the existence of invariant sets. This way in [2] a method of a classification of images relating to a substance propagation process was proposed. The image is considered as a lattice formed by pixels of given intensities. Then the oriented graph corresponding to the image is constructed by the following way. The number of vertices is equal to the number of pixels. Every vertex has the weight equal the pixel intensity. It is connected with its neighbours (depending on neighbourhood type), and all the edges outcoming from the vertex have the value of its weight divided on the number of neighbours. The constructed flow is normed. Hence we obtain Markov chain on the graph: for every vertex its weight equals sum of weights of outcoming edges. Denoting the initial distribution on graph edges by p_{ij} we find such a distribution u_{ij} that the flow on the graph be stationary: for every vertex the sum of weights of incoming edges equals the sum of weights of outcoming ones. It is well known that such a problem has a solution if there is a cycle on a graph. Moreover, this solution minimizes weighted entropy $g(u) = -\sum_{i,j} u_{ij} \ln \frac{p_{ij}}{u_{ij}}$. It is weighted entropy that is used as a classifying sign when images relating to different doses of a substance are analyzed. In fact, weighted entropy may be considered as a time that is required for a distribution process to achieve a stationary state.

If a given image has complex multifractal structure we may assume that there are several distributions on this set. Each of them may be obtained as the solution of an extremum problem for Regny entropy. It is worth noting that namely on this way of reasoning one can obtain the connection between Regny spectrum and multifractal spectrum [6]. In literature this connection is known as the Legendre transform [21].

Images with different structures may have identical entropy characteristics, because the entropy does not depend on the order of component in a probability distribution vector, and this order defines the structure of the image. For example two Serpinsky carpets constructed by different methods

but having the same number of black and white cells have the same entropy. (It is interesting to note that they have the same similarity dimensions).

In such cases it is reasonably to use Regny divergences (called also α-divergences). We note that by analogy with fractal dimension we should calculate a set of Regny divergences for more accurate analysis and classification. The advantages of such a technic are demonstrated in [11] when analyzing images with different structures.

The results of many studies convincingly show that when analyzing digital images the dealing with a vector of signs leads to more accurate results. For example, in [18] the authors applied *fractal signature* method to analyze textures. It is based on the construction of a sequence of special *blankets* [6] for the image and calculation a numerical characteristic (fractal signature) which is closely connected with the Minkovsky dimension. Every such a blanket corresponds to an image obtained from a given one by resolution changing. The vector of fractal signatures is the image characteristic, and the distance between two images may be defined as the Euclidean distance between their vectors. In [3] the method was successfully applied to classify the biomedical preparations images of 4 classes.

In this work we propose to obtain a vector characteristic of an image which is constructed by the following way. We consider both a given measure distribution and its direct multifractal transform [21], which is a renormalization of the given measure. Such transforms form a group, and the set of measures is the group transitivity class. For two given distributions we construct their direct multifractal transforms and calculate Kullback-Leibler divergences between both initial distributions and their renormalizations. The obtained divergence vectors may be considered for comparing given images.

The method is illustrated by the Serpinsky carpet example. For two methods of the carpet construction we obtain the sets having the same entropy, but Kullback-Leibler divergence between them is nonzero. Moreover, we obtain the estimation of Kullback-Leibler divergence on *k*th step of direct multifractal transform that shows that the divergence grows as a linear function of *k*. Numerical experiments were performed for images from Brodatz album (presented both in grayscale and HSV palette). Our method successfully distinguishes textures that have close structures. The images from two classes of biomedical preparations (presented both in grayscale and HSV palette) were studied as well. In every class the average divergence vector on every color component was calculated. Experiments showed that for different classes the rates of growth of these vectors are substantially different, that allows considering them rates as a classifying sign.

2 Main concepts

2.1 Regny entropies

Let a discrete probability distribution $p = \{p_i\}$, $p_i \geq 0, \sum p_i = 1,\ i = 1,...,n$ be given. Following [4] we define the Regny entropy of order α as

$$H_\alpha(p) = \frac{1}{1-\alpha} \ln \sum_1^n p_i^\alpha. \qquad (1)$$

It is known [13] that the entropy is nonincreasing function of α. When α tends to 1 the Regny entropy turns into Shannon entropy. The most generally used Regny entropies are

$H_0(p) = \ln n$ (Hartley entropy),

$H_1(p) = -\sum_1^n p_i \ln p_i$ (Shannon entropy),

$H_2(p) = -\ln \sum_1^n p_i^2$,

$H_\infty(p) = -\ln \max_i p_i$ (min-entropy). (2)

It is easy to note that entropy characteristics do not depend on the position of components p_i in the distribution vector p. In other words, using them one cannot distinguish between two images with different structures but having the same number values p_k.

2.2 Regny divergences

Let p and q be discrete probability distributions. Define Regny (or α -) divergences as

$$D_\alpha(p,q) = \frac{1}{\alpha - 1} \ln \sum_1^n p_i^\alpha q_i^{1-\alpha}. \qquad (3)$$

The Kullback-Leibler divergence (for α =1) is defined as

$$D_1(p,q) = \sum_1^n p_i \ln \frac{p_i}{q_i}. \qquad (4)$$

2.3 Direct multifractal transform

Consider a distribution $p = \{p_i\}$ that defines some measure on the image and consider the following

direct multifractal transform $f_k(p) = \dfrac{p_i^k}{\sum_i p_i^k}$ [21].

It is easy to understand that such transforms form a group, because

$f_{k_1} \circ f_{k_2} = f_{k_1 k_2}$,

$f_k \circ Id = f_k$,

$f_k \circ f_{1/k} = Id$,

$Id = f_1$.

Every transform results in a renormalization of the initial measure and we can consider a new image relating to the transform. The set of measures is the group transitivity class. Hence we analyze not only initial image, but a set of its modifications as well.

For a given p we denote the measure obtained by means of f_k as $p(k)$. In [21] the author considers the set of Kullback-Leibler divergences between the initial measure p and $p(k)$, namely

$$D_1(p, p(k)) = (1-k)\sum_i p_i \ln p_i + \ln \sum_i p_i^k .$$

Hence the obtained vector is a characteristic of the image by means of the initial measure transform, and may be used for different images comparing. However, for two types of the Serpinsky carpet these vectors turn to be the same.

2.4 Divergences between direct multifractal transforms

Consider the following method to compare distributions p and q. We construct their multifractal transforms $p(k)$ and $q(k)$, and calculate

$$D_1(p(k), q(k)) = \sum_i \frac{p_i^k}{\sum_i p_i^k} \ln \frac{p_i^k}{\sum_i p_i^k} \frac{\sum_i q_i^k}{q_i^k} . \quad (5)$$

As a result we obtain a sequence of Kullback-Leibler divergences for a given initial measure and its transforms. This vector is a characteristic of the class transitivity of the group. For different initial measures their transitivity classes are different, hence this vector may be used as a classifying sign.

3 Example: Serpinsky carpet

Consider the following example. Let us construct the Serpinsky carpet (the first step) by two ways. We take unit square, divide every side onto 7 parts and obtain 49 small squares. Then delete 9 small squares as shown on Fig.1.

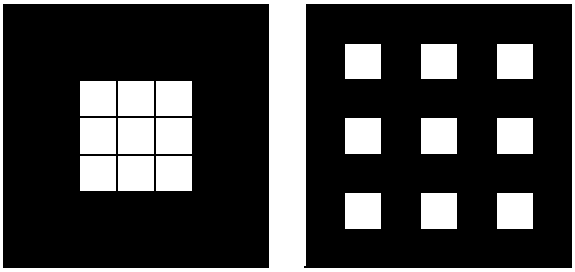

Fig. 1 Two types of the Serpinsky carpet (the first step of the construction)

We see that the obtained images have different structures. According to (1) entropy characteristics do not allow distinguishing between the images. In addition, as it was marked in [12], these images have the same similarity dimension, namely $D_s = \dfrac{\ln 40}{\ln 7}$.

In this case the distribution vector is the union of vectors constructed on the first step. Hence the entropy characteristics will be the same.

In what follows we need some denotations. Let us suppose that for the Serpinsky carpet the normalized intensity (measure) of a small black square is b, and the measure of white square is w, so that $40b + 9w = 1$. We suppose that w is a small number and $b = wm$, where m is a real number.

To calculate the Kullback-Leibler divergence for the example we have to find the sum of divergence between rows of the matrix constructed in accordance with images: every square is coded by b or w. Divergences for 1 and 7 rows are equal zero, because the rows are identical. Denoting the divergence in k_{th} rows by $D_1^k(p,q)$ we have

$$D_1^2(p,q) = 3b \ln m, D_1^3(p,q) = -3w \ln m,$$

$$D_1^4(p,q) = 2(b-w) \ln m, D_1^5(p,q) = -3w \ln m,$$

$$D_1^6(p,q) = 3b \ln m .$$

So,

$$D_1(p,q) = 8(b-w) \ln m \quad (6)$$

and two types of the Serpinsky carpet are different images.

On the second step on the Serpinsky carpet construction we have to repeat the described procedure for every of black squares. The results are shown on Fig. 2 (Figure after [17].)

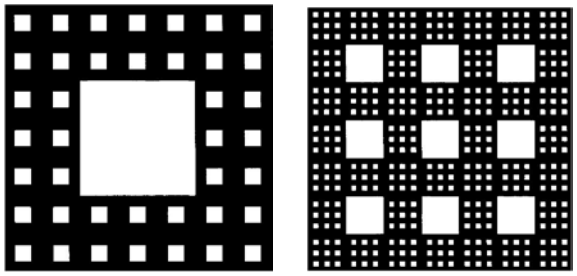

Fig. 2 Two types of the Serpinsky carpet (the second step of the construction)

Taking into account the results for the first step it is not difficult to obtain that the Kullback-Leibler divergence is equal to 72/49* $D_1(p,q)$.

Now we perform direct multifractal transform and calculate the divergences in accordance with (5).

For the Serpinsky carpets $\sum_i p_i^k = \sum_i q_i^k$, because the images have the same number of black and white squares. By (6) for initial distribution we have

$$D_1(p,q) = 8b(1-\frac{1}{m})\ln m.$$

In this case (5) has the form

$$D_1(p(k),q(k)) = \frac{k}{\sum_i p_i^k}\sum_i p_i^k \ln\frac{p_i}{q_i}.$$

By using (6) we have

$$\sum_i p_i^k \ln\frac{p_i}{q_i} = 8b^k(1-\frac{1}{m^k})\ln m,$$

and finally

$$D_1(p(k),q(k)) = \frac{8k}{u_k}(1-\frac{1}{m^k})\ln m,$$

where $u_k = 40 + \frac{9}{m^k}$.

For k large enough

$$D_1(p(k),q(k)) \approx \frac{k}{5}\ln m,$$

i.e. the divergence increases proportionally to k.

4 Numerical experiments

The experiments were performed for textures from a standard test set (Brodatz textures, [23]) and for images of biomedical preparations. The choice of the size of a partition box depends on the size of a given image. It should be noted that for any image the smaller the box size the more the Kullback-Leibler divergence is. But experiments show that the results are similar for different box sizes: for close textures the divergence vector grows insignificantly, but for different structures it grows rather fast. Hence we chose box size depending on the image size — 50x50 for Brodatz textures and 100x100 for biomedical preparations images.

4.1 Images from the Brodatz album

To verify the proposed algorithm we use texture from the set of Brodatz textures, both for grayscale and colored images. All the images have size 640x640 pixels. The size of a partition box is 50x50. Our experiments show that the method results in good separation of different images. Below we give the results of calculation of the divergence vector between pictures D78 and D79 when they are given in gray scale and in color. The colored images are presented in RGB palette. We also used HSV palette. On Fig. 3 the images D78 (a) and D79 (b) in grayscale are given. Table 1 shows the divergence vector between them.

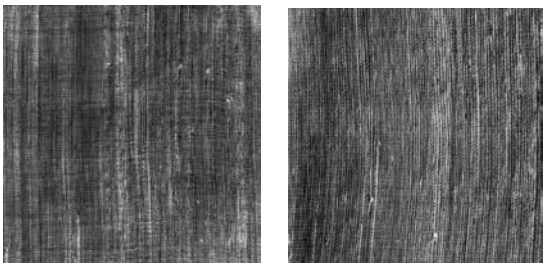

a b

Fig. 3 Images D78 (a) and D79 (b) in gray scale

k	$D_1(p(k),q(k))$
1	0,017049
2	0,017049
3	0,067669
4	0,151078
5	0,266670
6	0,414185
7	0,593832
8	0,806294
9	1,052580
10	1,333669
11	1,649993

Table 1. Divergence vector for images D78 and D79

On Fig. 4 the same images are given in RGB palette, and tables 2 and 3 show the divergence vectors calculated in RGB and HSV palettes

component wise.

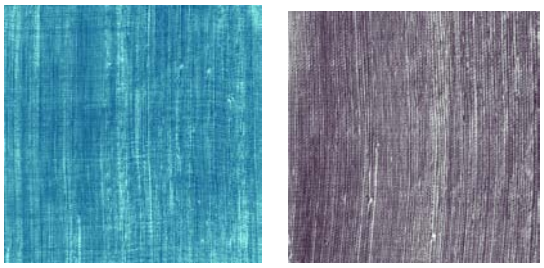

a b

Fig. 4 Images D78 (a) and D79 (b) in RGB palette

k	$D_1(R)$	$D_1(G)$	$D_1(B)$
1	0,015394	0,008653	0,003876
2	0,061776	0,034376	0,015479
3	0,139415	0,076780	0,034738
4	0,248687	0,135476	0,061557
5	0,390258	0,210109	0,095827
6	0,565166	0,300391	0,137435
7	0,774654	0,406108	0,186274
8	1,019675	0,527137	0,242240
9	1,300092	0,663434	0,305240
10	1,613808	0,815033	0,375189

Table 2. Divergence vectors for each component of RGB palette

k	$D_1(H)$	$D_1(S)$	$D_1(V)$
1	0,000889	0,019703	0,004105
2	0,003553	0,079310	0,016407
3	0,007974	0,179190	0,036850
4	0,014121	0,319025	0,065358
5	0,021953	0,497670	0,101842
6	0,031426	0,713158	0,146214
7	0,042495	0,962840	0,198389
8	0,055114	1,243614	0,258294
9	0,069237	1,552172	0,325862
10	0,084821	1,885218	0,401040

Table 3. Divergence vectors for each component of HSV palette

4.2 Biomedical Preparations Images

Experiments were performed for two classes of biomedical preparations images: healthy and chronic pyelonephritis kidneys, being each class contains 12 images. The images were obtained by microscope AxioCam MRc5 of the company Carl Zeiss Microimaging GmbH. All the images were made with 200-fold zoom, represented in RGB and have size 2584x1936 pixels.

A preliminary classification was performed by an expert. The size of partition cell is 100x100. All the images are represented both in grayscale and HSV palette (component wise).

At first we compare two images from different classes: left picture (health kidney) is supposed to have the distribution p, and right picture (kidney with pyelonephritis) — q. The results of calculation in grayscale are given below.

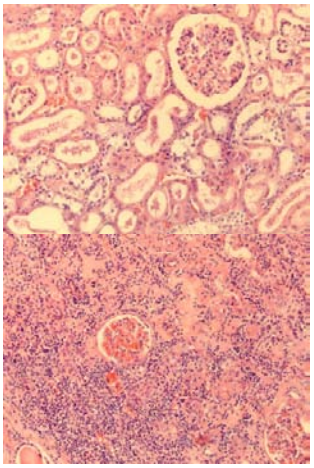

a b

Fig. 5 Healthy kidney (a) and kidney with chronic pyelonephritis (b)

k	$D_1(p(k),q(k))$
1	0,004716
2	0,003112
3	0,012435
4	0,027942
5	0,049594
6	0,077345
7	0,111138
8	0,150907
9	0,196580
10	0,248079
11	0,305319

Table 4. Divergence vector for images from different classes

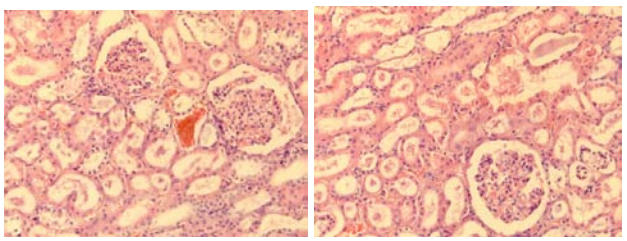

Fig. 6 Two images of healthy kidney

On Fig. 6 the images belonging to the class of healthy kidneys are shown. The results in Table 5 demonstrate that for images with similar structures the divergences vector grows more slowly.

k	$D_1(p(k), q(k))$
1	0,000221
2	0,001309
3	0,005241
4	0,011801
5	0,020994
6	0,032820
7	0,047279
8	0,064366
9	0,084076
10	0,106399
11	0,131323

Table 5. Divergence vector for images from the same class

4.3 Divergence vectors for a class

Hence we may use a rate of the divergence vector growth as a classification sign for a class of images. For two classes of images (each contains 12 elements) we calculated divergence between pairs (i,i+1), (where i=1..11) of images and using them obtained the average vector (DA) – the vector of arithmetical means. As experiments show, the change of the comparison order does not effect on the divergence significantly, hence we do not take into account comparisons in order (i+1,i). Calculation were performed for each component of HSV palette. Class of images of healthy kidney is denoted by class0, and the images of kidney with pyelonephritis – class1.

In the table below results of calculation for class0 are given.

k	$DA(H)$	$DA(S)$	$DA(V)$
1	0,025537	0,000669	0,000165
2	0,102807	0,002678	0,000657
3	0,231442	0,006028	0,001468
4	0,409872	0,010727	0,002590
5	0,635992	0,016786	0,004016
6	0,907214	0,024225	0,005738
7	1,219883	0,033064	0,007750
8	1,568659	0.043336	0,010045
9	1,946487	0,055075	0,012616
10	2,345339	0,068326	0,015457

Table 6. Components of DA vector for the class0

Below we show the results for the class of kidney with chronic pyelonephritis images.

k	$DA(H)$	$DA(S)$	$DA(V)$
1	0,161711	0,002897	0,002943
2	0,540739	0,011607	0,011643
3	1,047320	0,026194	0,025896
4	1,637891	0,046767	0,045493
5	2,288850	0,073479	0,070219
6	2,986059	0,106519	0,099860
7	3,720182	0,146113	0,134202
8	4,484515	0,192516	0,173036
9	5,273950	0,246013	0,216158
10	6,084430	0,306904	0,263371

Table 7. Components of DA vector for the class1

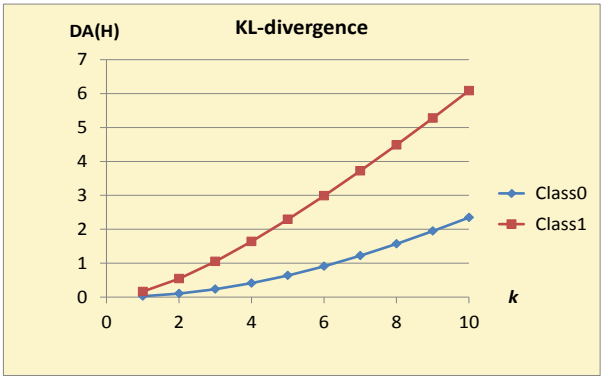

Fig.7 Comparing DA vectors – H component

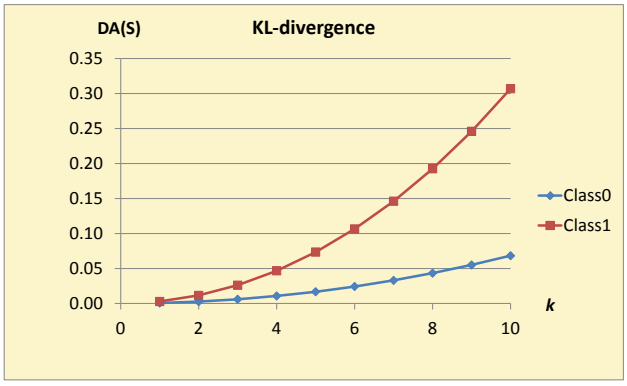

Fig.8 Comparing DA vectors – S component

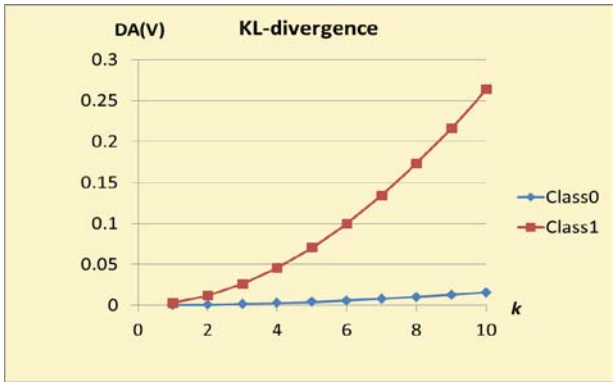

Fig.9 Comparing DA vectors — V component

5 Conclusion

The described method is a natural generalization of the Kullback-Leibler divergence application. We consider not only an initial distribution of pixel intensities, but the distributions obtained by the group of multifractal transforms. Hence we obtain an additional set of images which is connected with a given one. By considering modifications of a given image we use additional information and obtain more grounded classification sign — the growth rate of the average divergence vector for a class. For different classes these vectors are substantially different (as in gray scale as in any component of RGB and HSV palettes), which allows applying the proposed method to analyze and classify complex textures.

Acknowledgment

Authors wish to express their thanks to the staff of the department of morbid anatomy of Mariinsky hospital in St. Petersburg for providing the images of biomedical preparations, and V. Sergeev for help in numerical experiments. This work was supported in part by the Russian Foundation of Basic Research (RFBR) under Grant 13-01-00782.

References:

[1] A. S. Abdul-Nasir, M. Y. Mashor, Z. Mohamed. “Colour image segmentation approach for detection of malaria parasites using various color models and k-mean clustering”, WSEAS Transaction on Biology and Biomedicine, vol. 10, no. 1, 2013, pp. 41-55.

[2] N. B. Ampilova, “Stationary processes on graphs and image analysis”, Computer instruments in education, no. 3, pp. 27-32, 2013 (in Russian).

[3] N. Ampilova, I. Soloviev, Y. Shupletzov, “On some aspects of the fractal signature method”, in Proc. 8th Int. Conf. CEMA13, Sofia, 2013, pp. 80-84.

[4] A. Bashkirov, “Regny entropy as a statistical entropy for complex systems”, Theoretical and Math. Physics, 149(2), 2006, pp.299-317 (in Russian).

[5] A. Chhabra, C. Meneveau, R. Jensen and K.R. Sreenivasan, “Direct determination of the f(α) singularities spectrum and its application to fully developed turbulence”, Physical Review A, vol. 40, no. 9, November 1, 1989. pp. 5284-5294.

[6] K. J. Falconer, Fractal Geometry. Mathematical Foundations and Applications. John Wiley & Sons, 1990.

[7] A. Feher, A. Bekefi, Szilvia Nagy, “Structural entropy based processing of colorectal polyp images”, in Proc. 8th Int. Conf. CEMA13, Sofia, 2013, pp. 44-47.

[8] R. Gonzalez, R. Woods. Digital Image Processing, Prentice Hall, 2002.

[9] R. M. Haralick, K. Shanmugom, I. Dinstein. “Textural features for image classification”, IEEE Transaction on systems, man and cybernetics, vol. SMC-3, no. 6, 1973. pp. 610-621.

[10] R. M. Haralick. ”Statistical and Structural Approaches to Texture”, Proceedings of the IEEE, vol.67, no. 5, 1979, pp. 786-804.

[11] Alfred O. Hero, Bing Ma, Olivier Michel, and John Gorman, “Alpha-Divergence for Classification, Indexing and Retrieval”, Communications and Signal Processing Laboratory, Technical Report CSPL-328, May 2001, available at http://www.eecs.umich.edu/ ˜hero.

[12] D. L. Jaggard, A. D. Jaggard and P. Frangos, “Fractal Electrodynamics: Surfaces and Superlattices”, in Frontiers in Electromagnetics, D. H. Werner and Raj Mittra, Eds., IEEE Press, 2000, pp. 1-47.

[13] P. Jizba, T. Arimitsu, “The world according to Rényi: Thermodynamics of multifractal systems”, Annals of Physics (Elsevier), 312, 2004, pp. 17–59.

[14] H. Kim, R. Poltayev, B. Hong, “An intrinsic image representation and its application to left ventricle segmentation in cardiac MRI images”, Journal of Medical Imaging and Health Information, vol. 4, no. 4, 2014, pp. 612-620.

[15] E. Lim Wei Jie, "Automated detection of mild glaucoma stage using grayscale features of fundus images", Journal of Medical Imaging and Health Information, vol.4, no. 2, 2014, pp. 267-271.
[16] A. Malamou, A. Karakasiliotis, E.Kallitsis, G. Boultakadis and P.Frangos, "An autofocusing algorithm for postprocessing of synthetic aperture radar (SAR) images based on image entropy minimization", Proc. 7th Int. Conf. CEMA12, Sofia, 2012, pp.53-56.
[17] B. B. Mandelbrot, The Fractal Geometry of Nature, Freeman, San Francisco, 1983.
[18] S. Peleg, J. Naor, R. Hartley, D. Avnir, "Multiple Resolution Texture Analysis and Classification", IEEE transactions on pattern analysis and machine intelligence, vol. PAMI-6, no. 4, 1984. pp. 518-523.
[19] J. Serra. Image Analysis and Mathematical Morphology, Acad. Press, London, 1982.
[20] M. Tuceryan, Anil K. Jain, Texture analysis, in The Handbook of Pattern Recognition and Computer Vision (2nd Edition), by C. H. Chen, L. F. Pau,P. S. P. Wan, Eds., pp. 207-248, World Scientific Publishing Co., 1998.
[21] G. Vstovsky, Elements of information physics. Moscow, MGIU, 2002.
[22] Y. Xu, H. Ji, C. Fermüller, "Viewpoint Invariant Texture Description Using Fractal Analysis", International Journal of Computer Vision, no. 83, 2009, pp. 85–100.
[23] http://multibandtexture.recherche.usherbrooke.ca/original_brodatz.html